Dark energy from α-attractors: phenomenology and observational constraints

Carlos García-García,[a,b] **Eric V. Linder,**[c,d] **Pilar Ruíz-Lapuente**[a,b] **and Miguel Zumalacárregui**[c,e]

[a]Instituto de Física Fundamental, Consejo Superior de Investigaciones Científicas, c/. Serrano 121, E–28006, Madrid, Spain

[b]Institut de Ciències del Cosmos (UB–IEEC), c/. Martí i Franqués 1, E–08028, Barcelona, Spain

[c]Berkeley Center for Cosmological Physics and Berkeley Lab, University of California, Berkeley, CA 94720, USA

[d]Energetic Cosmos Laboratory, Nazarbayev University, Astana, Kazakhstan 010000

[e]Institut de Physique Théorique, Université Paris Saclay CEA, CNRS, 91191 Gif-sur-Yvette, France

E-mail: carlosgarcia@iff.csic.es, evlinder@lbl.gov, pilar@icc.ub.edu, miguelzuma@berkeley.edu

Abstract. The possibility of linking inflation and late cosmic accelerated expansion using the α-attractor models has received increasing attention due to their physical motivation. In the early universe, α-attractors provide an inflationary mechanism compatible with Planck satellite CMB observations and predictive for future gravitational wave CMB modes. Additionally α-attractors can be written as quintessence models with a potential that connects a power law regime with a plateau or uplifted exponential, allowing a late cosmic accelerated expansion that can mimic behavior near a cosmological constant. In this paper we study a generalized dark energy α-attractor model. We thoroughly investigate its phenomenology, including the role of all model parameters and the possibility of large-scale tachyonic instability clustering. We verify the relation that $1 + w \sim 1/\alpha$ (while the gravitational wave power $r \sim \alpha$) so these models predict that a signature should appear in either the primordial B-modes or in late time deviation from a cosmological constant. We constrain the model parameters with current datasets, including the cosmic microwave background (Planck 2015 compressed likelihood), baryon acoustic oscillations (BOSS DR12) and supernovae (Pantheon compressed). Our results show that expansion histories close to a cosmological constant exist in large regions of the parameter space, not requiring a fine-tuning of the parameters or initial conditions.

Contents

1 Introduction

In the last few years, different inflationary models were realized to yield similar values for the primordial scalar perturbation ratio, n_s, and the gravitational wave tensor to scalar ratio, r, for a wide range of inflation potentials. These models predict that for N e-folds of inflation, up to leading order [1]

$$n_s = 1 - 2N^{-1} \quad \text{and} \quad r = 12N^{-2}\,, \tag{1.1}$$

being compatible with WMAP [2] and Planck [3] cosmic microwave background (CMB) observations. The reason why all of them have similar predictions is a second order pole in the kinetic coefficient of the Einstein frame Lagrangian; i.e. with no coupling to the Ricci scalar and a non-canonical kinetic coefficient for the scalar [1]:

$$\mathcal{L} = \sqrt{-g}\left[\frac{1}{2}M_P^2 R - \frac{\alpha}{(1-\varphi^2/6)^2}\frac{1}{2}(\partial\varphi)^2 - \alpha f^2\left(\frac{\varphi}{\sqrt{6}}\right)\right]\,, \tag{1.2}$$

where M_P is the Planck mass, α is a parameter and αf^2 is the potential function. This Lagrangian is obtained from an inflationary multifield Lagrangian with a locally conformal transformation symmetry, once the extra degree of freedom associated to this symmetry is gauge fixed and the potential function f is required to be real [4].

The field redefinition $\phi = \sqrt{6\alpha}\,\mathrm{arctanh}(\varphi/\sqrt{6})$ makes the scalar field's kinetic coefficient canonical, allowing to write the theory as a quintessence model

$$\mathcal{L} = \sqrt{-g}\left[\frac{1}{2}M_P^2 R - \frac{1}{2}(\partial\phi)^2 - \alpha f^2(x)\right]\,, \tag{1.3}$$

where $x = \tanh(\phi/\sqrt{6\alpha})$. Now, the field space is expanded in the connected region of φ since this transformation pushes the limits of the original field, $\varphi \in (-\sqrt{6}, \sqrt{6})$, towards $\pm\infty$ in the transformed field, $\phi \in (-\infty, \infty)$.

In the dark energy context, α-attractors have been gaining attention due to their possibility for linking both inflationary and present accelerated expansions. In the same way as their predictions in inflation are in good agreement with the latest cosmological observations, as quintessence models they can also produce a late accelerated expansion compatible with present measurements. Their potential connects power law scalar field potentials near the minimum $x = 0$ to a cosmological constant, in the form of a plateau as $x \to \infty$. A series of works based on this idea have appeared recently. The connection of both cosmological epochs is studied in Ref. [5], where a particular potential with two plateau regimes allows both inflation and a near cosmological constant expansion. This work was extended in Ref. [6] by computing the reheating era and setting constrains on the model parameter space (see also [7]).

Concentrating on late time acceleration and the α-attractors as dark energy, Ref. [8] related these models to the thawing and freezing classes of dark energy and generalized the two most common forms of the potential to a unified form, which we will use here. Other works have also examined the dark energy applications, e.g. [9, 10].

Other investigations include the use of α-attractors for dark matter [11], and the relation of α-attractors with $f(R)$ gravity, extending the original connection of α-attractors with Starobinsky R^2 gravity [12], e.g. [13, 14].

We focus here on testing the α-attractor dark energy model against different cosmological observations and physical understanding of the constraints on the parameter space. We use the generalized potential of Ref. [8] and allow the initial field value to vary, since fixing it restricts the phenomenology and can bias the results. Furthermore, we will thoroughly investigate the dependence of the model on each parameter and its initial value conditions showing that cosmological constant-like solutions are generic and do not require any fine-tuning of the model parameters and initial conditions. In addition, we will investigate the tachyonic instabilities noted in Ref. [8] to see if there is any signatures of interesting phenomenology, such as clustering dark energy, and if they can cause an observable imprint.

In Section 2, we briefly review the model proposed in Ref. [8] and carefully examine the theory dependence on each parameter (Sections 2.1 and 2.2). We investigate in Section 2.3 how the observables change with the model parameters, including a quantitative assessment of the tachyonic instability phenomenon in terms of an observable signature. In Section 3 the model is confronted against observational data from CMB Planck 2015 [15], baryon acoustic oscillation (BAO) DR12 [16], and the supernove Type Ia distances in terms of binned $E(z) = H(z)/H_0$ [17]. Section 3.1 describes these datasets and why we chose them, while in section 3.2 we present the priors to be used in the Bayesian study of the next two subsections. In section 3.3, we compare the Starobinsky form of the potential with ΛCDM, leaving just one parameter (the scaling α itself) free in order to assess if this form, and the Starobinsky value $\alpha = 1$ is favored. In Section 3.4 we then free every parameter to obtain the full α-attractor generalized model posterior distribution. We conclude in Section 4.

2 The model

We will work on the generalized α-attractor potential from [8]. In the language of equation 1.3, $V(\phi) = \alpha f^2(x)$ is the field potential and, in this case, is given by

$$V(x) = \alpha c^2 \frac{x^p}{(1+x)^{2n}} = \alpha c^2 2^{-2n} (1-y)^p (1+y)^{2n-p} \,, \tag{2.1}$$

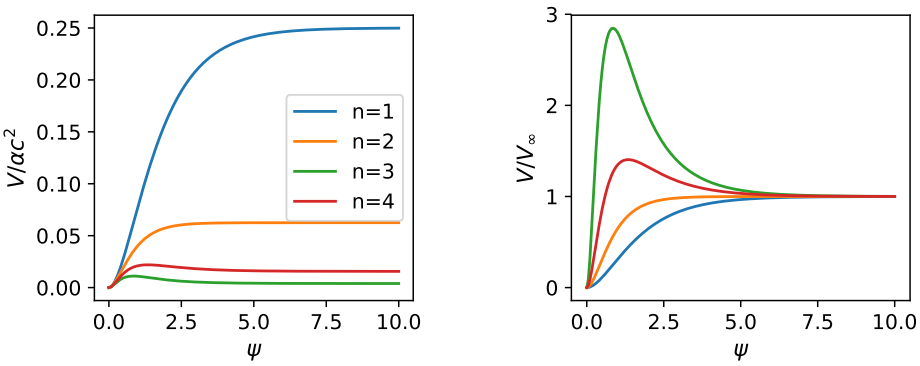

Figure 1: Generalized α-attractor potential for different values of n, fixing $p = 2$. For $n > 2$, there is a maximum. The maximum strengthens with n if the potential is normalized to its asymptotic amplitude.

with c, p, n constant parameters and $y \equiv e^{-2\phi/\sqrt{6\alpha}}$. The case $\alpha = 1$, $n = 1$, $p = 2$ corresponds to the Starobinsky model [18–20], working in natural units, i.e. reduced Planck mass $M_P = 1$ and speed of light, $c = 1$. We will work on a flat geometry motivated by inflation. Figure 1 shows the potential for different values of n using the variable $\psi \equiv \phi/\sqrt{\alpha}$, the scaled scalar field, since it is actually what determines the value of $V(x)$. Note how n controls the transition from the flat plateau to the monomial-shaped minimum.

Let us briefly summarize the potential properties before studying thoroughly the dependence on each parameter. The potential interpolates from a power law potential with index p to a cosmological constant fixed value, basically an uplifted (negative) exponential potential, for positive values of the field:

$$V(|\psi| \ll \sqrt{6}) \approx \alpha c^2 6^{-p/2}\, \psi^p \ , \tag{2.2}$$

$$V(\psi \gg \sqrt{6}) \approx \alpha c^2\, 2^{-2n} \left[1 - 2(p-n)\, e^{-2\psi/\sqrt{6}}\right] \xrightarrow[\psi\to\infty]{} \frac{\alpha c^2}{2^{2n}} \ . \tag{2.3}$$

We see that the amount of dark energy in the Universe will be determined by the potential amplitude, αc^2. Note there is no true cosmological constant: the potential is zero at the minimum.

The α-attractor potential has a maximum at $x_{\rm max} = p/(2n-p)$ given $n > p$ [8]. Fields starting (from rest) at $x > x_{\rm max}$ will roll towards infinity and the asymptotic constant potential, i.e. a de Sitter solution, while asymptotically freezing. On the other hand, for $x < x_{\rm max}$ the field would roll toward the origin along the plateau and eventually (possibly in the future) down toward the zero minimum. However, if it rolls too far off the plateau the kinetic energy rises, forcing the equation of state w far from -1 and it would not be a viable dark energy model today. Therefore we are not concerned with fields rolling past the minimum and so only need to deal with positive field values. Fields with $x < x_{\rm max}$ basically act like thawing models; they depart from a cosmological constant like behavior.

So far we have talked about the known properties of this model, already studied in Ref. [8]. Now, we will start our detailed study on its dependence on each parameter. We will vary α, n and p. The parameter c is fixed by the closure relation $1 = \sum_i \Omega_i$, where Ω_i is the fractional energy density, i.e. the ratio of the energy density of component i (e.g. matter,

dark energy, radiation) to the critical density. To solve the field evolution

$$\ddot{\phi} + 3H\dot{\phi} + V_\phi = 0 \ , \tag{2.4}$$

where $V_\phi = dV/d\phi$, we also need to specify the initial value of the field ϕ_{ini} and its velocity $\dot{\phi}_{ini}$. For a field starting on the nearly flat plateau (and if it starts off the plateau it is not using the α-attractor characteristics) the Hubble friction will freeze the field at early times (we start at $z_{ini} = 10^{14}$ in the radiation era) and so we take $\dot{\phi}_{ini} = 0$. Thus ϕ_{ini} is the only further parameter. To solve the coupled differential equations that govern the cosmological history we use the hi_class Boltzmann code[1] [21, 22].

2.1 Dependence on the scaling of the potential (α)

We start our study on the effect of the different parameters varying the simplest one: the scaling α. This has close connections with the underlying particle physics (e.g. supergravity or conformal field theory model). Note that α scales the field value and the potential amplitude, but cannot be removed by a field redefinition since it does not appear in the kinetic terms $\dot{\phi}^2/2$.

Generally, larger values of α bring the model closer to ΛCDM, as the potential dominates more over the kinetic energy and the plateau is stretched out longer for a given value of ψ. We can make this more quantitative by employing the flow formalism for a thawing field [23],

$$1 + w = \frac{4}{27}\left(\frac{V_\phi}{V}\right)^2 \Omega_{DE} + \mathcal{O}(V_{,\phi\phi}) \tag{2.5}$$

Since for fields on the plateau, $V_\phi/V \sim 1/\sqrt{\alpha}$, then $1 + w \sim 1/\alpha$. We have numerically checked this relation holds until quite recent times and plotted $(1 + w_0)\alpha$ in Figure 2. Note that in the quintessential inflation model of Ref. [7] they also find $1 + w \sim 1/\alpha$, while the CMB tensor to scalar ratio $r \sim \alpha$ so a physics signature is present either in r (if α is large) or w (if α is small). In addition, we can see that for thawing models the field evolution $(\psi_{ini} - \psi_0) \sim 1/\alpha$, where ψ_0 is the value today. This relation comes from

$$(\phi_0 - \phi_{ini}) = \int_{ini}^{0} dt\, \dot{\phi} \approx \int_{ini}^{0} dt\, \sqrt{\rho_{DE}(1 + w)}\,. \tag{2.6}$$

Since the dark energy density changes little for thawing models, one can see that $\sqrt{\alpha}(\psi_{ini} - \psi_0) \sim \sqrt{1 + w_0}$ [24]. Effectively, Figure 2 shows that for viable models (those with $w_0 < -0.8$) these relations hold quite well.

Note the initial value of the field plays an important role, with fields with high initial values mimicking the results of a cosmological constant. That is, $w_0 \approx -1$ and $\psi_{ini} - \psi_0 \approx 0$. This is seen in Figure 2. Note that when $p > n$ (here $p = 2$, $n = 1$), the potential does not have a maximum and the field will always roll down towards $\psi = 0$. However, sufficiently large initial fields stay on the plateau nearly frozen for the whole evolution history of the Universe. For initial values of the field closer to $\psi = 0$, the parameter α determines when the field starts rolling down and, as a consequence, how fast it moves and how far the equation of state parameter is from the cosmological constant solution. Larger α's slow the field down, keeping it closer to cosmological constant behavior.

[1] http://hiclass-code.net

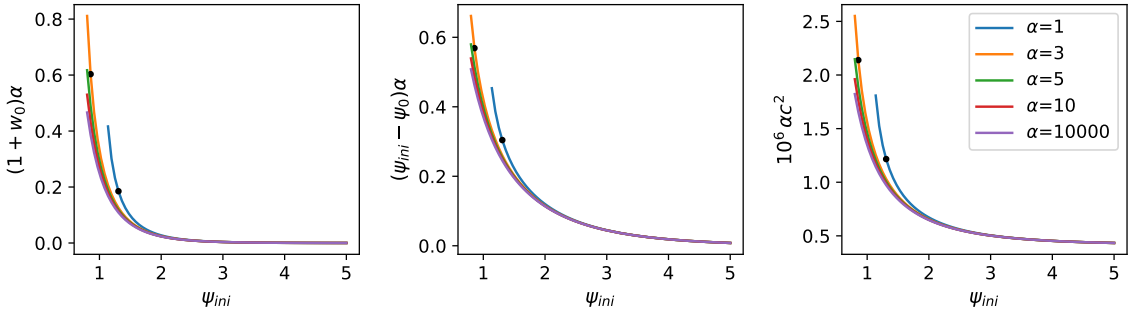

Figure 2: The dynamical quantities $(1 + w_0)\alpha$ and $(\psi_{ini} - \psi_0)\alpha$ are nearly independent of α for values of ψ_{ini} that deliver $1 + w_0 < -0.8$ (marked by black dots). Other parameters are fixed to $p = 2$ and $n = 1$, with c fixed by the density closure relation.

The case with $p < n$ has a maximum that causes a different phenomenology depending on the relative size of ψ_{ini} and ψ_{max} so that any field starting at high values ($\psi_{ini} > \psi_{max}$) would roll towards the de Sitter attractor. This case will be studied in detail in Section 2.2 and is shown in Figure 4.

Finally, the potential amplitude αc^2, responsible for the amount of dark energy in the Universe, which is kept fixed, needs to be adjusted to compensate the loss that comes from the evolving part of the potential, $V/\alpha c^2$. This is shown in the rightmost panel of Figure 2. It is fairly insensitive to ψ_{ini}, especially for large ψ_{ini} where the field stays nearly frozen. As Eq. (2.3) shows, once the amplitude is accounted for, the remaining form of the potential is insensitive to α, so the curves all lie together.

Thus, models will be close to ΛCDM if they either have large α (recall $1 + w_0 \sim 1/\alpha$) or large ψ_{ini}. Since allowing them to get larger and larger will give the same physical results, in Section 3.2 we pay careful attention to priors for the Monte Carlo analysis.

2.2 Dependence on the shape of the potential (p and n)

In this section we will study how the exponents, p and n, change the field evolution history. We treat them together because, leaving aside the low and high ψ regimes, where the potential is governed by, respectively, p and n separately (Equations 2.3 and 2.2), in the most interesting, intermediate ψ values it is their relative size that matters most.

For completeness, recall that p governs the low ψ regime (equation 2.2) as $V \propto \psi^p$, and the slope of the potential (for a given n) in the transition between the plateau and the power law regime. The field evolution will be faster and earlier with larger p. Nevertheless, this prescription is only valid in the low-ψ regime and in the case $p > n$. The case with $n > p$, which will be analyzed later, is different because of the appearance of a maximum, whose size, position and steepness is determined by their relative size. The only different case is $p = 0$ because it is the only configuration that exclusively allows the field to grow towards the de Sitter attractor, since the potential is monotonically decreasing. This analysis is confirmed by numerical solution of the evolution equations, as seen for $\alpha = 1$ and $n = 1$, in Figure 3.

The exponent n, instead, fixes the asymptotic behavior of $V(\psi)$ as $V \to \alpha c^2 2^{-2n}$ (equation 2.3) having a direct impact on the potential amplitude. This means that for a fixed amount of present dark energy density, the value of αc^2 must be modified in order to correct the deficit caused by n; thus it shifts up or down as seen in Figure 4.

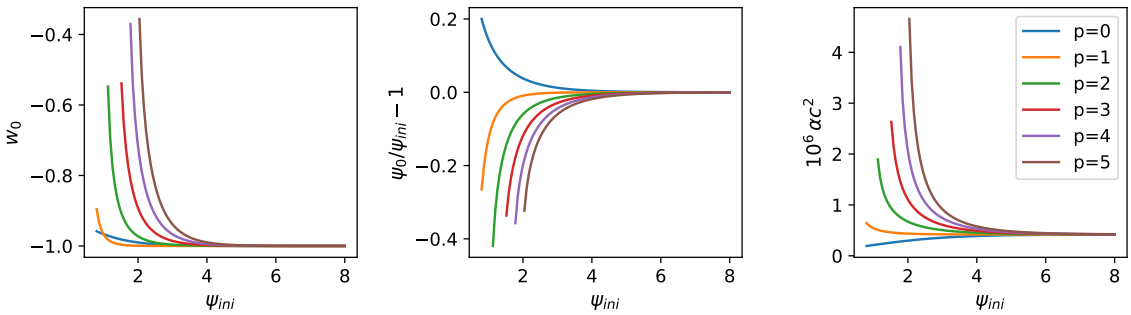

Figure 3: The values of w_0, $\psi_0/\psi_{ini} - 1$ and αc^2 are plotted vs ψ_{ini} for various values of p, for a fiducial model with $\alpha = 1$ and $n = 1$. Except for $p = 0$, for which the potential (equation 2.1) is monotonically decreasing, the exponent p determines the low-ψ shape of the potential. For $p \geq n$, the steepness grows with p, making the field evolve faster (and earlier). The potential amplitude αc^2 varies to compensate for the field evolution in order to preserve the same present dark energy density. Note that viable models with $w_0 < -0.8$ need small p or high ψ_{ini}.

We can also use figure 4 to study the interdependence of both exponents in the intermediate ψ values since $p = 2$ and n ranges from 0 to 5 so that there are solutions with $(p < n)$ and without $(p > n)$ a potential maximum. In the later case, the potential plateau is slightly inclined towards $V = 0$ and the transition regime that connects it with the power law regime is steeper as $p - n$ grows. This expression also governs the size, slope and position of the maximum when $n > p$. On the one hand, its position is given by $x_{max} = p/(2n - p)$, so that increasing n shifts the potential maximum toward $\psi = 0$. Quantitatively, for the studied cases with $n = 3, 4, 5$, the maximum is located at $\psi_{max} = 1.35, 0.85, 0.63$. On the other hand, fixing the dark energy content makes the peak higher and steeper: for $n = 3, 4, 5$ the ratio of the potential maximum to its asymptotic value is $V_{max}/V_\infty = 1.40, 2.84, 6.87$, respectively.

Thus, fields starting at $\psi_{ini} > \psi_{max}$ roll down toward ∞ with a velocity dependent on its proximity to the maximum. While fields with $\psi_{ini} \gg \psi_{max}$ remains almost frozen $(w_0 \sim -1)$ on the plateau, those with $\psi_{ini} \sim \psi_*$ (ψ_* is the inflection point at $\psi > \psi_{max}$), where the slope is maximal, speed up, departing from the cosmological constant solution (w_0 grows). For ψ_{ini} closer to ψ_{max} the field feels a weaker force and its evolution is slower (w_0 decreases), having as a limit case, $\psi_{ini} = \psi_{max}$, where the field remains frozen for the whole evolution history of the Universe $(w = -1)$. Starting at $\psi_{ini} < \psi_{max}$ the field rolls down again, but this time toward $\psi = 0$. The closer to the minimum it starts, the faster it evolves (w_0 grows quickly). Note that the shift in the maximum reduces the available space at $\psi_{ini} < \psi_{max}$ as n grows, e.g. giving the shift of the minimum to the left in Figure 4.

2.3 Model Predictions and Observables

Now we will focus on the phenomenological predictions of the model given by equation 2.1. Besides the effects on the background expansion, in Ref. [8] it was suggested that, as a consequence of having $m^2 = V'' < 0$ near the edge of the plateau, one might find some interesting phenomenology, such as clustering dark energy. The field perturbations $\delta\phi_k$ in

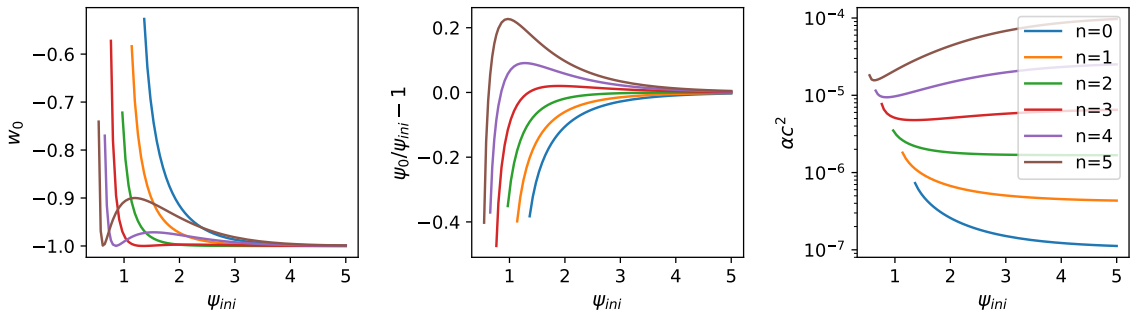

Figure 4: As Figure 3 but varying with respect to n, with a fiducial model $\alpha = 1$ and $p = 2$. All curves end at the lowest value that gives $\Omega_{DE} \sim 0.7$ today. The relative size of n respect to p changes the potential slope on the plateau: the closer they are, the less pronounced the slope is. This means that as n goes to $p = 2$, the field rolls down later and slower. The potential amplitude αc^2 varies to compensate for the amplitude reduction 2^{-2n} in Equation 2.3 in order to preserve the same present dark energy density. Note that viable models with $w_0 < -0.8$ need $n \approx p$ or high ψ_{ini}.

momentum space becomes [25]

$$\delta\ddot{\phi}_k + 3H\delta\dot{\phi}_k + \left(\frac{k^2}{a^2} - m^2\right)\delta\phi_k = 4\dot{\phi}_k\dot{\Phi} - 2V_{,\phi}\Phi\,, \tag{2.7}$$

in standard Newtonian gauge notation, where the metric perturbations $\Phi = \Psi$.

Since perturbations start growing significantly at horizon entering, we will just consider $k > H$ modes. In addition, equation 2.7 tell us that the mass term must be $|m^2| \gtrsim k^2/a^2$ in order to change the perturbation growth, bounding the scales sensitive to the imaginary mass to

$$\frac{|m^2|}{H^2} \gtrsim \frac{k^2}{a^2H^2} > 1\,. \tag{2.8}$$

Given that the field starts evolving at late times ($z \sim O(1) - O(10)$) and that the field's mass will not be extremely high, the affected wavenumber will be $k \approx 10^{-3}\,\mathrm{Mpc}^{-1}$, i.e. much larger scales than where precision clustering data lies. In addition, late time evolution implies that perturbations will not have much time to grow.

As a consequence, observing some effect requires a sufficiently large negative mass squared. We have computed the present value of the mass squared term for each model studied in the previous section, and plotted it in figure 5. One can read from it that models with exponents $n < p$ have only two regions, separated by the inflection point in the transition zone, so that $m^2 < 0$ is expected for high ψ_{ini} and $m^2 > 0$ at low ψ_{ini}. On the contrary, as $n > p$ implies the appearance of a maximum, the region with $m^2 < 0$ is bounded by the inflection points. It is important to remark that, given that n makes the maximum steeper as it grows, high n can give rise to sufficiently negative m^2, which, in theory, could be potentially noticeable. Nevertheless, for the sensible models studied here, with no extreme exponents, and compatible with the dark energy density observations, which in the end fixes the potential amplitude, we have found that all models have a similar perturbation growth, just varying a little bit close to the present.

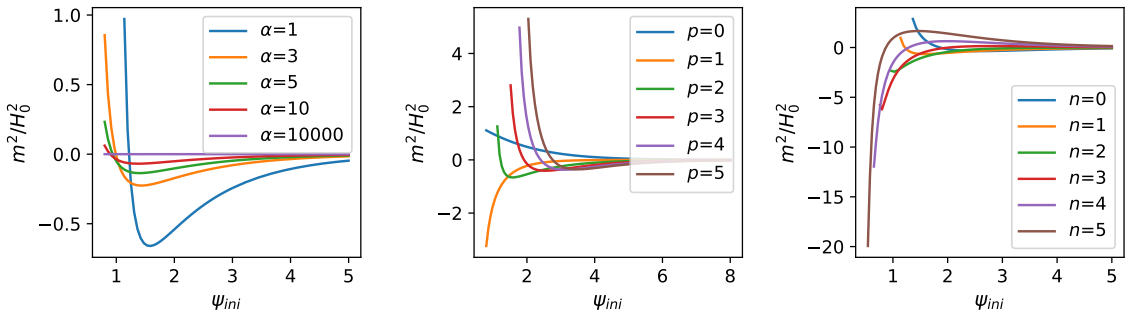

Figure 5: The mass squared m^2/H_0^2 can go negative, as is standard for hilltop models, but general not deeply (relative to H^2) or for long. When $n < p$, there are two regions, delimited by the inflection point in the transition between the power law regime and the plateau, where the mass squared is positive or negative, respectively. On the contrary, if $n > p$, the appearance of a maximum means that $m^2 < 0$ is bounded around it by the two inflection points. As commented in section 2.2, n has a great impact on the relative size of the maximum respect to the plateau, making it also the parameter with greatest impact on m^2.

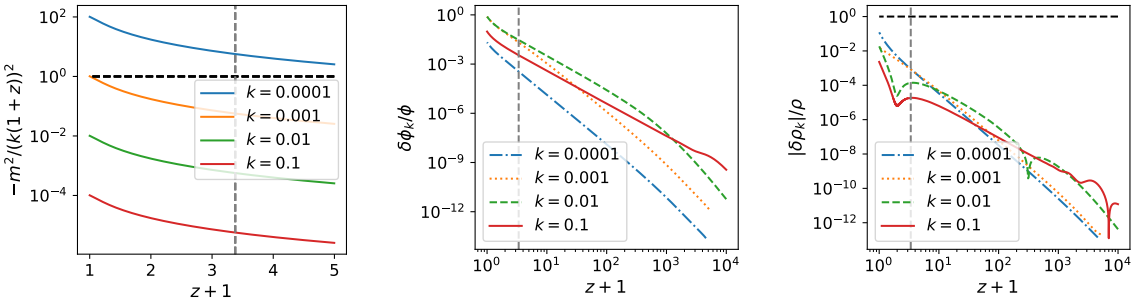

Figure 6: Redshift evolution is shown of the mass squared relative to the k^2/a^2 term (left), the normalized field perturbation (middle), and the normalized density perturbation for the model $\alpha = 1$, $\psi_{ini} = 0.542$, $p = 2$ and $n = 5$, the extreme model with $m_0^2/H_0^2 \approx -20$. The vertical dashed line marks the redshift when $|m^2|/H^2 = 1$ and the horizontal one shows $|\delta\rho_k/\rho| = 1$. k is in units of Mpc^{-1}. Recall that the mode with $k = 10^{-4}\,\mathrm{Mpc}^{-1}$ has not yet entered in the horizon. Dark energy density perturbation modes are negligible with respect to its background value during almost the whole evolution history even for this extreme model.

Figure 6 illustrates that even the extreme model with with $m^2/H_0^2 \sim -20$ (that indeed has unviable equation of state $w(a) \approx -0.74 - 1.9(1-a)$) shows that perturbations have little effect on the dark energy density or field value for the cosmic history up to the present.

Similarly, the growth function of matter perturbations (figure 7) does not show a significant change with respect to ΛCDM. Since the dark energy equation of state only deviates appreciably from -1 at low redshift, the growth factor is close to that of ΛCDM until recently. Only those models that roll significantly, falling off the plateau show more than percent level deviations.

In those cases, the matter power spectrum as shown in figure 8 is lowered as well,

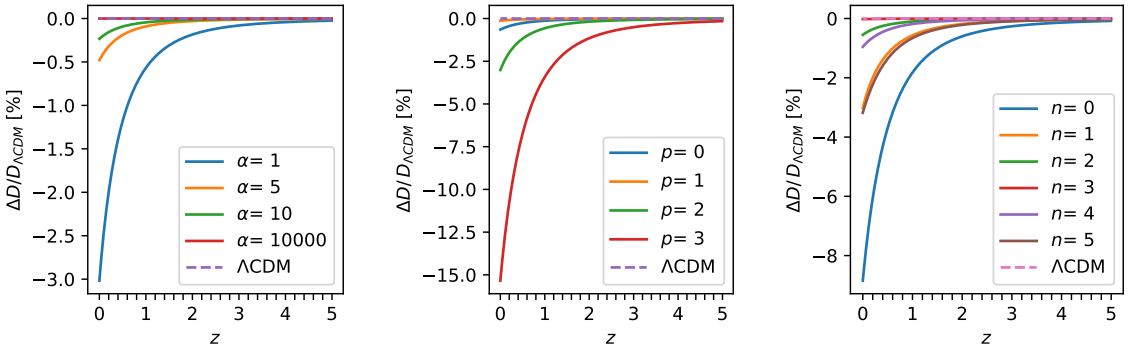

Figure 7: The matter density perturbation growth factor D is shown as the relative deviation from ΛCDM for different models varying α, p and n, using $\alpha = 1$, $p = 2$, $n = 1$ and $\psi_{ini} = 1.5$ as the base model. The more the field moves, the more thawing, allowing dark energy to dominate earlier, suppressing matter growth. By contrast, the case with $n = 3$ has the field frozen for $\psi_{ini} > 1$ and so $w_0 \approx -1$ (see the left panel of figure 4). Higher ψ_{ini} would freeze most models in the plateau, decreasing deviations from ΛCDM.

yielding relative differences up to a few percent. Similarly the CMB temperature angular power spectrum (figure 9) departs from ΛCDM. Such deviations can be compared with experimental data letting us rule some models out. In particular, the larger differences at high multipoles are due to the geometric shift in the distance to recombination, anticipating that CMB and BAO galaxy distances will be important to take into account.

Distances are integrals over the Hubble parameter, i.e.

$$D_A = \frac{1}{1+z}\int_0^z \frac{dz'}{H(z')}\,, \tag{2.9}$$

for the flat universe we consider. While the Hubble parameter should have its largest deviation from from ΛCDM at low redshift, as an integral the distance has increasing deviation with redshift. These quantities are shown in figure 10 and figure 11. Thus we expect that both $z < 3$ measures, e.g. from supernovae and BAO, and high redshift measures from the CMB, will play important roles in constraints.

3 Observational constraints

In this section we will compare the α-attractor model (equation 2.1) with recent observations. In section 3.1 we will explain the choice of datasets based on the knowledge acquired in previous sections. Then, in section 3.2, we will impose some appropriate and sensible priors which will be needed in the study of the posterior distributions of two iconic cases: that with the exponents of the Starobinsky model ($p = 2$, $n = 1$) but with the scaling allowed to be free, and that with all the parameters freed. We will see that a large portion of the parameter space is ruled out, favoring models close to ΛCDM.

3.1 Data sets

We will use the Planck 2015 observations [15], BAO DR12 [16] and the measurements of $E(z) = H(z)/H_0$, obtained using the latest SN Ia at $z > 1.5$ [17, 26]. The reason we choose

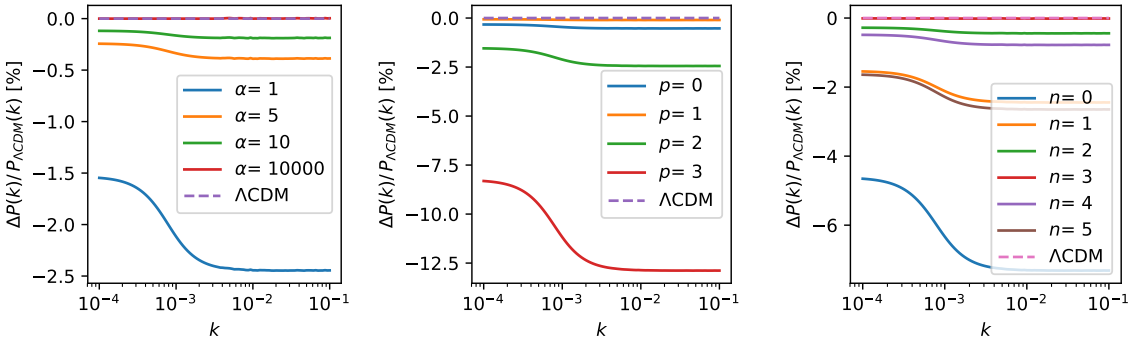

Figure 8: The matter power spectrum $P(k)$ is shown as the relative deviation from ΛCDM for different models varying α, p and n, using $\alpha = 1$, $p = 2$, $n = 1$ and $\psi_{ini} = 1.5$ as the base model. The more the field thaws, the more the power spectrum is suppressed.

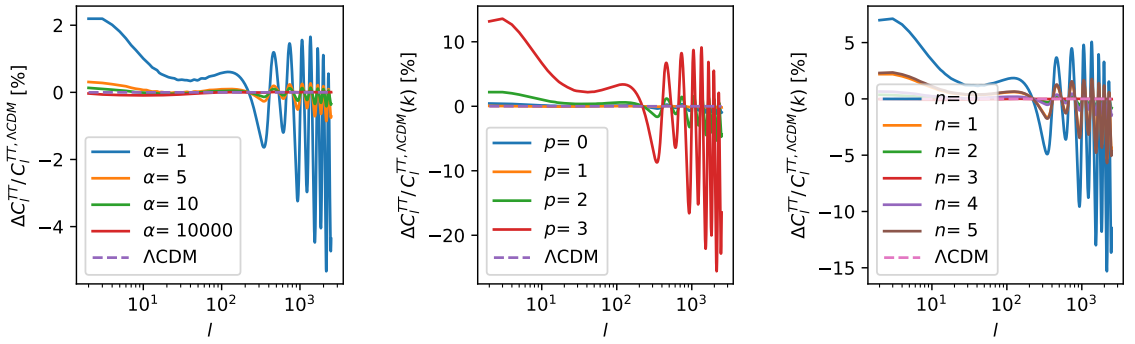

Figure 9: Temperature angular power spectrum (C_l^{TT}) is shown as the relative deviation from ΛCDM for different models varying α, p and n, using $\alpha = 1$, $p = 2$, $n = 1$ and $\psi_{ini} = 1.5$ as the base model. Apart from having different amplitude for low l, the spectrum is shifted in angular scale with respect to that of ΛCDM.

these observations is that Planck sets high redshift constraints, although it also take into account the lower redshift effects through integration, BAO does at low redshift, where we have found the largest differences, and $E(z)$ imposes direct constraints in the expansion rate up to $z = 1.5$.

In general, CMB observations are used because CMB is affected by the expansion rate, the matter components and inflationary conditions (a good summary of reasons is found in section 2 of [15]), allowing the constriction of the cosmological parameters. Indeed, for models close to ΛCDM it allows precise evaluation of them. Furthermore, since deviations from ΛCDM on the power spectrum rise up to few percents (figures 8 and 9), Planck and BAO likelihoods could be sensitive to them. BAO set low redshift constraints on H and $D_M = (1 + z)D_A$, where the models' greatest differences with respect to ΛCDM are found. We have chosen the latest released dataset, BAO DR12 [16], which covers $z \lesssim 0.7$. We have not used Lyman-α BAO measurements, even though they go much deeper in redshift, because they are in tension with Planck and low redshift BAO measurements [27, 28]. For instance,

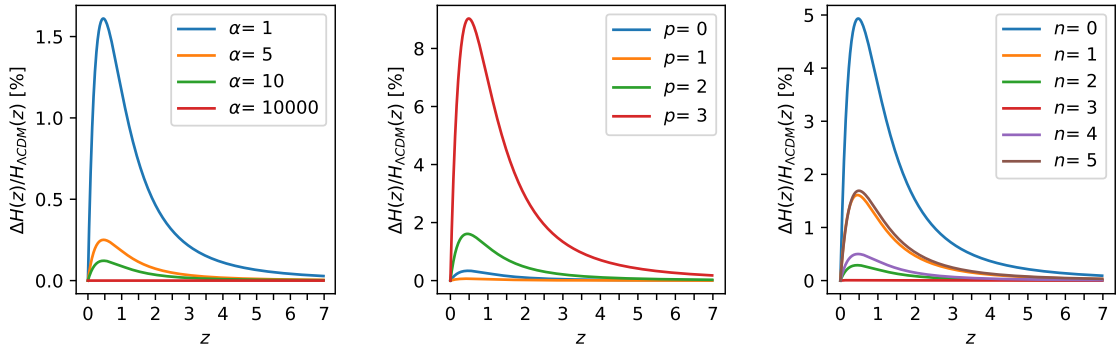

Figure 10: Hubble parameter is shown as the relative deviation from ΛCDM for different models varying α, p and n, using $\alpha = 1$, $p = 2$, $n = 1$ and $\psi_{ini} = 1.5$ as the base model. Fields that thaw more have larger expansion rates, modulo the normalization to fixed H_0 today.

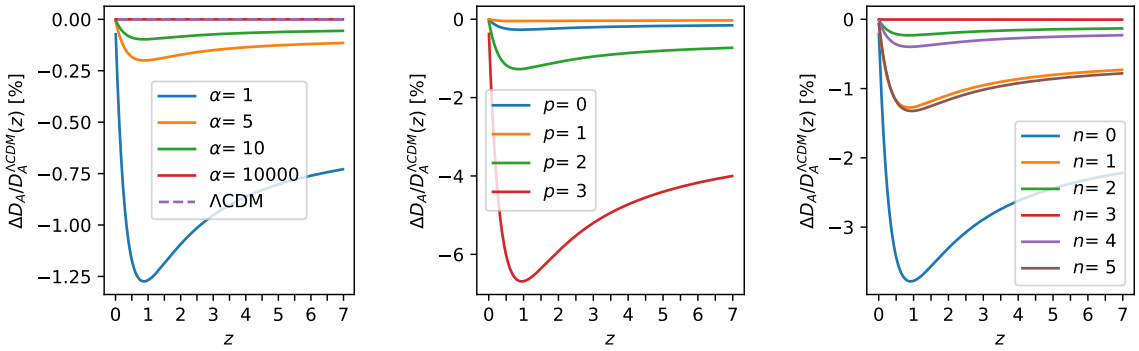

Figure 11: Angular distance is shown as the relative deviation from ΛCDM for different models varying α, p and n, using $\alpha = 1$, $p = 2$, $n = 1$ and $\psi_{ini} = 1.5$ as the base model.

in ΛCDM the discrepancy is approximately 2σ, and our model is phenomenologically too close to ΛCDM to avoid the tension. Lastly, further control on the expansion rate is given by the estimates of $E(z)$ up to $z = 1.5$ using the SN Ia distance observations at $z > 1.5$ [17, 26].

We compute only the background quantities due to their dominance over perturbations (figure 6), which, additionally, were seen to be not very constraining (figures 8 and 9) and require much more computation time. The cases of figure 9 that show the most deviation in perturbation observables are actually ruled out from the acoustic scale (l_A values are off by 22, 66, and 42σ respectively). The acoustic scale is well accounted for in the Planck compressed likelihood we use, that compresses most of the power spectrum information in the following three background-dependent variables (and the scalar spectral index), given in table 4 of Ref. [15]:

- The CMB shift parameter [29], R,

$$R \equiv \sqrt{\Omega_m H_0^2} D_M(z_*)/c \ = 1.7488 \pm 0.0074\,. \tag{3.1}$$

- The angular scale of the sound horizon at last scattering

$$l_A \equiv \pi D_M(z_*)/r_s(z_*) = \pi/\Theta_* = 301.76 \pm 0.14\,. \tag{3.2}$$

- The baryon density: $\Omega_b h^2 = 0.02228 \pm 0.00023$.

We recall that $D_M = (1+z)D_A$, i.e. the comoving distance to redshift z, where z_* is the redshift for which the optical depth is unity, $r_s(z_*) = r_*$ is the comoving size of the sound horizon at z_* and $h = H_0/(100\,\mathrm{Mpc}^{-1}\mathrm{km\,s}^{-1})$. The Planck collaboration checked that the reduced likelihood is in good agreement with the full one for ΛCDM and wCDM. Since our models of interest lie close to ΛCDM, these approximations should serve well.

BAO DR12 measurements [16] are independent of Planck's and are in good agreement with them. Since the most deviating cases are ruled out from the acoustic scale, we can just consider the background quantities and use the consensus BAO-only values suggested in the paper. We have taken them from its electronic archive[2]. Let us note that the actual variables that BAO can measure are $D_M(z)/r_d$ and $H(z)r_d$, which take into account changes in the cosmological parameters and in the pre-recombination energy density era. Since r_d is the sound horizon at drag epoch (z_d), $r_d = \int_{z_d}^{\infty} dz\, c_s(z)/H(z)$, with c_s the speed of sound, and our models are nearly identical to ΛCDM at high redshift, the BAO data informs us of deviations in D_M and H.

Finally, $E(z)$ constraints [17] compress the information of a thousand SN Ia distances from the unreleased Pantheon dataset and Hubble Space Telescope, including 15 new discovered supernova at redshift $z > 1.5$. Their measurements are thought to be precise and unbiased estimates of $E(z)$ as long as the expansion rate does not vary much nor have localized features between the specific chosen redshifts, as for our model. Their only assumptions were flatness, not mandatory but convenient, and continuity and smoothness of $E(z)$ in order to parametrize its inverse by its values at different specific redshifts. They used those points to interpolate and recover the whole function, necessary to compute the luminosity distance (equation 2.9), which they could compare against their selection of well-calibrated SN data.

3.2 MCMC setup

The posterior distribution of the α-attractor model (equation 2.1) which will be shown in next section has been obtained by sampling the parameter space with a Markov chain Monte Carlo (MCMC) method. In particular, we made use of MontePython [30] and CosmoHammer [31] which embeds emcee [32], an implementation of the Goodman and Weare affine invariant ensemble sampler [33]. We chose this algorithm instead of the traditional Metropolis-Hasting to avoid acceptance rate and convergence problems since affine invariant sampling methods are uniformly effective over all the convex bodies with same space dimension and regardless of their shape [33]. In addition, CosmoHammer parallelization allows much faster computations.

The priors are summarized in table 1. Since the parameters for viable models do not vary over much more than an order of magnitude, and no particular values are preferred, a uniform prior is reasonable. This matches well with the MontePython implementation of CosmoHammer which does not allow informative or unbounded priors. As we have seen in section 2, sufficiently high values of the scaling α or the initial field ψ_{ini} all yield ΛCDM-like universes. Also, the exponents, p and n, just under the condition of being close to each other,

[2] https://data.sdss.org/sas/dr12/boss/papers/clustering/ALAM_ET_AL_2016_consensus_and_individual_Gaussian_constraints.tar.gz

Parameter	Range
H_0	[40, 90]
$\Omega_b h^2$	[0, 0.04]
$\Omega_{cdm} h^2$	[0, 0.3]
$\dot{\phi}_{ini}$	$\{0\}$
ψ_{ini}	[0, 3.5]
α	[0, 10]
p	[0, 10]
n	[0, 10]
c	Fixed by $1 = \sum_i \Omega_i$

Table 1: Priors used in the MCMC posterior inference. H_0 units are $[\mathrm{km\,s^{-1}Mpc^{-1}}]$ and c is obtained by a bijection method.

no matter how high they were, yield more ΛCDM-like results provided that the field had not started rolling off the plateau too early, i.e. the viable set of models. There is therefore no point in allowing a large range of such high values, which all give essentially ΛCDM. Therefore we bound their space to prevent walkers[3] wasting time in the infinite ΛCDM regime, although we set the bounds large enough to be able to explore all the interesting phenomenology of the model. Finally, in order to accelerate the convergence, we fixed c with the closure relation $1 = \sum_i \Omega_i$, using a bijection method.

3.3 Starobinsky form vs ΛCDM

Before studying the full general model posterior distribution, we want to focus on the more constrained case with exponents $p = 2$ and $n = 1$, the one which reduces to the Starobinsky potential when the scaling $\alpha = 1$. Increasing the parameter space in stages will let us understand more easily how the model behaves, letting us check our understanding of its dependence on α and ψ_{ini}. Furthermore, the scaling acts as an interpolation between the ΛCDM (high ψ_{ini} or α) and Starobinsky models ($\alpha = 1$).

After studying the autocorrelation times, we decided to use 70 walkers per varied parameter, i.e. 350 walkers in total, and run 300 iterations, from which we discarded half of them as burn in. Fewer iterations would have sufficed since the slowest autocorrelation function crosses 0 around 70, but we took a conservative approach given the low time cost. To analyze convergence we used the MontePython [30] internal routine which puts all chains together, ordered by iteration step, splits the resulting chain in three and calculates the Gelman-Rubin test.

The posterior distributions are shown in figure 12 while the quantitative results are in table 2. The first thing to note is that the cosmological parameters are in good agreement with ΛCDM Planck 2015 results [34]. This is related to the fact that our model has a preferred ΛCDM-like regime. In fact, we see that their posterior distribution is unaffected by α and almost any ψ_{ini}. The ψ_{ini} posterior distribution, however, has a lower boundary which sets $\psi_{ini} > 1.31$ at 95.4% confidence level. This value is altered by the parameters range choice, as we will see in next section, and cannot be understood as a general condition. The α-ψ_{ini} figure confirms what we said in section 2.1: the lower α and ψ_{ini} regime is disfavored as a

[3] A walker is the equivalent of a chain in a Metropolis-Hasting algorithm, in Goodman-Weare terminology. Note their dynamics are different, though.

consequence of the fact that a faster evolution of the field yields, for models that match the present dark energy density, a less negative equation of state, which is in tension with data. On the contrary, large α and ψ_{ini} freeze the field evolution getting it closer to $w = -1$, which the data prefer.

The dark energy equation of state parameters w_0 and w_a confirm our previous comments. Their values are close to $w = -1$, regardless of the particular value of α and ψ_{ini}. Again, the reason why this happens is that a large value of either one of them can give $w \approx -1$ (see for instance the $\alpha = 10^4$ case in figure 2).

The correlation between w_0 and w_a follows the typical pattern of thawing fields. In figure 13a, we have plotted the $w_0 - w_a$ posterior distribution over a random sample of 2×10^4 points colored as a function of the value of the present field mass. Those models with greatest probability follow the thawing relation $w_a \approx -1.6(1 + w_0)$ [24]. This leads to tight constraints on w_a. A more subtle effect is the correlation between the equation of state parameters and the field mass, which makes lower mass squared field models be located under those with higher mass squared for the same w_0. Recall that negative mass squared tends to occur for low α models, which also have greater deviations from $w = -1$.

The amplitude parameter c, which we have obtained by requiring $1 = \sum_i \Omega_i$, does not vary much; basically to get $\Omega_{de,0} \sim 1$, one requires $c^2 \lesssim H_0^2$, hence $c^2 \sim 10^{-7}\,\mathrm{Mpc}^{-2}$. This will change once we let n vary since n affects the height of the plateau and c must compensate any change on the potential to obtain the correct dark energy density. (Note that the best fit is actually slightly above the one dimensional confidence region; this is because there is much more parameter volume below the best fit values of ψ_{ini} and α, so lower values of c^2 are also more common in the full dimensional space.) Finally, the present field mass squared, m_0^2/H_0^2, is also constrained to be smaller in amplitude than ~ 0.4 (at 95% CL), and so tachyonic instabilities should not play an observable role, given the small effect of even $m^2/H_0^2 \approx -20$ in section 2.3.

Before moving to full model we note that the best-fit Starobinsky form model has $\alpha = 9.98$, far from the exact Starobinsky model of $\alpha = 1$. which is the actual Starobinsky potential. However, the χ^2_{min} difference is small, for one more parameter, and the Akaike Information Criterion [35], $\mathrm{AIC} = \chi^2 + 2k$, where k is the number of model parameters, tells us that neither of them is favored over the other ($\mathrm{AIC}_{BF} - \mathrm{AIC}_{\alpha=1} = -0.7$). Since the best fit α is at the prior upper bound, this is basically saying that ΛCDM is consistent with the data (recall that $1 + w_0 \sim 1/\alpha$).

3.4 Analysis of the full posterior distribution

Finally, we will study the general case with free exponents p and n, as well as α. It will collect all the dependencies we have been describing and let us find the full posterior distribution for the dark energy model proposed by Ref. [8], an α-attractor quintessential model with potential given by equation 2.1.

For this case the number of walkers per parameter was decreased to 60, giving a total of 420 walkers, the sample iterations were increased to 650, with 300 burn in iterations to be discarded, and 350 iterations to be stored. The extra degrees of freedom had a direct impact on convergence, making it much slower. As before, we checked the autocorrelation time and computed the Gelman-Rubin test with MontePython [30].

The results are written in table 3. In figure 14 we have plotted the marginalized posterior distribution of the model parameters and the present mass field, leaving aside the cosmological parameters because of their similarities with the results in previous section, represented in

Parameter	best-fit	best-fit with $\alpha = 1$	95% limits
$\Omega_{cdm}h^2$	0.1172	0.1171	$0.1173^{+0.0018}_{-0.0018}$
H_0	66.86	66.59	$66.83^{+0.79}_{-0.79}$
$10^2\Omega_b h^2$	2.225	2.223	$2.227^{+0.038}_{-0.037}$
ψ_{ini}	3.45	2.46	> 1.31
α	9.98	1.00	—
$10^7 c^2$	6.3	0.62	< 6.0
w_0	-0.996	-0.999	$-1 \leq w_0 < -0.962$
w_a	-6.00×10^{-3}	-1.72×10^{-3}	$0 > w_a > -0.0649$
m_0^2/H_0^2	-0.285	-0.042	$-0.099^{+0.31}_{-0.32}$
χ^2_{min}	15.741	17.073	—
χ^2_{min}/d.o.f.	0.984	1.067	—

Table 2: Parameter best fit values and 95% confidence limit for the $p = 2$, $n = 1$ Starobinsky form, allowing α to vary. The $\alpha = 1$ column corresponds to the pure Starobinsky model. H_0 units are $\mathrm{km\,s^{-1}Mpc^{-1}}$ and Mpc^{-2} for c^2. Note that α is unbounded at 95% CL (see figure 12).

figure 12. Note that the $\alpha - \psi_{ini}$ plot continues to show that ψ_{ini} and the kinetic coefficient α cannot be simultaneously small. Apart from that, all the parameter subspaces tell us something new. For example, the high exponent p disfavors the lower ψ_{ini} regime. As we said in section 2.2, higher p makes the low ψ_{ini} regime steeper, making the field roll faster and changing the expansion rate too much to match the observations. Higher n, changing more the amplitude of the plateau, do not have as strong an effect on the ψ_{ini} range, but does allow for much lower c; note that $n \sim 5$ in the middle of its range can suppress c^2 by a factor $2^{-2n} \sim 1000$.

However, we see that actually it is the difference $p - n$ that mostly matters (see equation 2.3 and section 2.2), with a strong correlation in the p vs n plane. The mean posterior, with the 95.4% CL values, is $p - n = -0.5^{+6.5}_{-5.5}$. Of course, higher values of ψ_{ini} and α make the constraint on $p - n$ weaker as they freeze the field so there is less sensitivity to the shape of the potential.

The $w_0 - w_a$ distribution (figure 13) is also broader and again follows the thawing solution, even better than before since allowing $p \approx n$ can give flatter plateaus.

It is important to note that introducing two new parameters has not improved the χ^2 ($\chi^2_{full} = 15.701 \simeq 15.741 = \chi^2_{np,fixed}$). This makes the Akaike Information Criterion ($|\Delta\mathrm{AIC}| = 4$) prefer the simpler model with fixed exponents. This result is a consequence of the data preferring ΛCDM, which can be reproduced just with high α or ψ_{ini}. Indeed, the best fit model is quite close to ΛCDM, having $(w_0, w_a) = (-0.998, -0.003)$.

3.5 Future observational data sets

Future experiments will be able to test in more detail the expansion histories of the α-attractors models studied in this paper that differ more subtly from the ΛCDM cosmological constant predictions. Using BAO measurements, we will have additional empirical information on the Hubble parameter $H(z)$ and the angular distance determinations D_A. From SN Ia we will obtain distance luminosity determinations D_L at various redshifts.

The Dark Energy Spectroscopic Instrument (DESI) will be a highly constraining BAO experiment. DESI will use four target classes from redshift z > 0.5 to z < 4 [36]. Those include

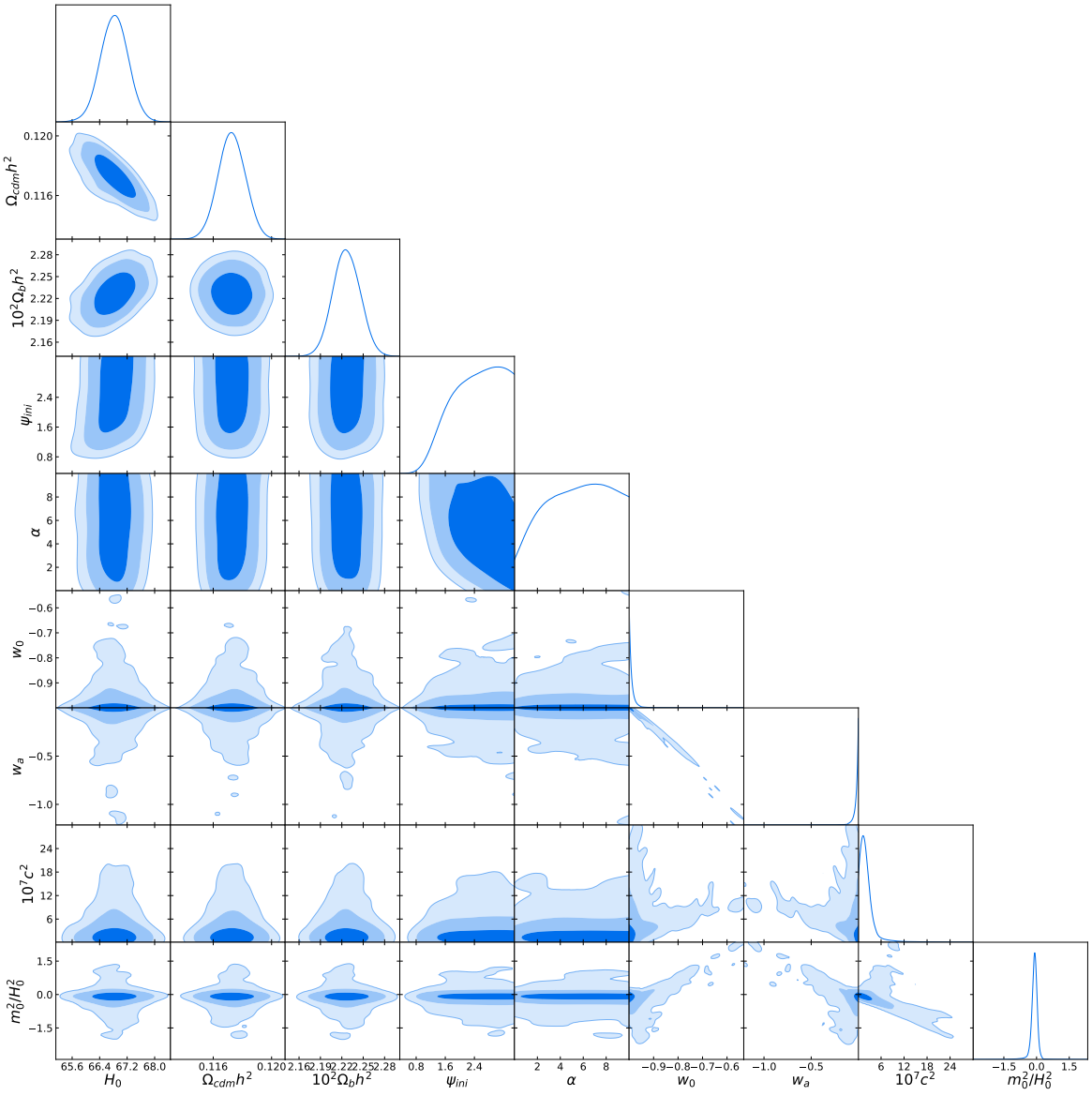

Figure 12: Posterior distributions for the Starobinsky form allowing α to vary, with $p = 2$, $n = 1$. The contours show the 68.3%, 95.5%, and 99.7% confidence levels, with darker colors for more probable results. The quantitative results are summarized in table 2.

Luminous Red Galaxies (LRGs), Emission Line Galaxies (ELGs), QSO and Lyman–alpha QSOs. In addition to the BAO measurements, this experiment will be able to discriminate models through growth rate of structure, with a precision comparable to that from weak lensing, through the redshift–space–distortions (RSD) method, which requires a very good sampling of the large scale structure. The Euclid satellite will also give highly accurate measurements for $z \gtrsim 1$ [37].

The WFIRST satellite will measure the expansion history of the Universe using supernovae. WFIRST will obtain thousands of well observed SN Ia and it is possible that it will observe SNe Ia identified by other telescopes such as the Large Synoptic Survey Telescope

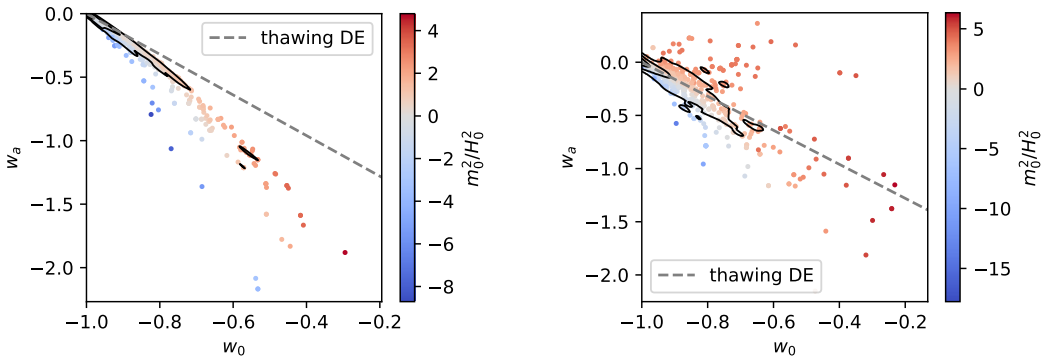

(a) Starobinsky-like ($p = 2$, $n = 1$). (b) General.

Figure 13: The w_0–w_a joint posterior distribution is shown for the Starobinsky form (left) and full generalized α-attractor (right) dark energy models (equation 2.1) over a random sample of 2×10^4 points colored depending on their present field mass. The dashed grey diagonal line represents the usual $w_0 - w_a$ relation for thawing models ($w_0 < -0.8$) described in reference [24].

Parameter	best-fit	mean ± 95% limits
$\Omega_{cdm}h^2$	0.1176	$0.1173^{+0.0019}_{-0.0019}$
H_0	66.79	$66.74^{+0.83}_{-0.88}$
$10^2\Omega_b h^2$	2.220	$2.227^{+0.037}_{-0.038}$
ψ_{ini}	2.962	> 0.952
α	3.803	—
$10^3 c^2$	1.84×10^{-2}	< 3.57
p	2.871	—
n	3.545	—
$p - n$	-0.7	$-0.5^{+6.6}_{-5.5}$
w_0	-0.998	$-1 \leq w_0 < -0.953$
w_a	-0.003	$-0.020^{+0.083}_{-0.077}$
m_0^2/H_0^2	-0.75	$-0.01^{+0.97}_{-0.87}$
$-\ln \mathcal{L}_{\min} = 7.850$, $\chi^2_{min} = 15.701 = 0.981$ d.o.f.		

Table 3: Best fit model for the full potential 2.1. H_0 units are $\mathrm{km\,s^{-1}Mpc^{-1}}$ and Mpc^{-2} for c^2. Note that α, p and n are unbounded (see figure 14).

(LSST) [38]. The growth of structure of the Universe will be also obtained by WFIRST.

These are all very powerful cosmological tools to discriminate between the candidates studied here against other physical models of dark energy.

4 Conclusion

We have studied the α-attractor dark energy model proposed in Ref. [8], and expressed in equation 2.1, inspired by the α-attractor class of inflationary models. It is a generalization of the well known Starobinsky potential which correspond to the case with kinetic coefficient $\alpha = 1$ and exponents $p = 2$ and $n = 1$, with no coupling to matter since it is not obtained

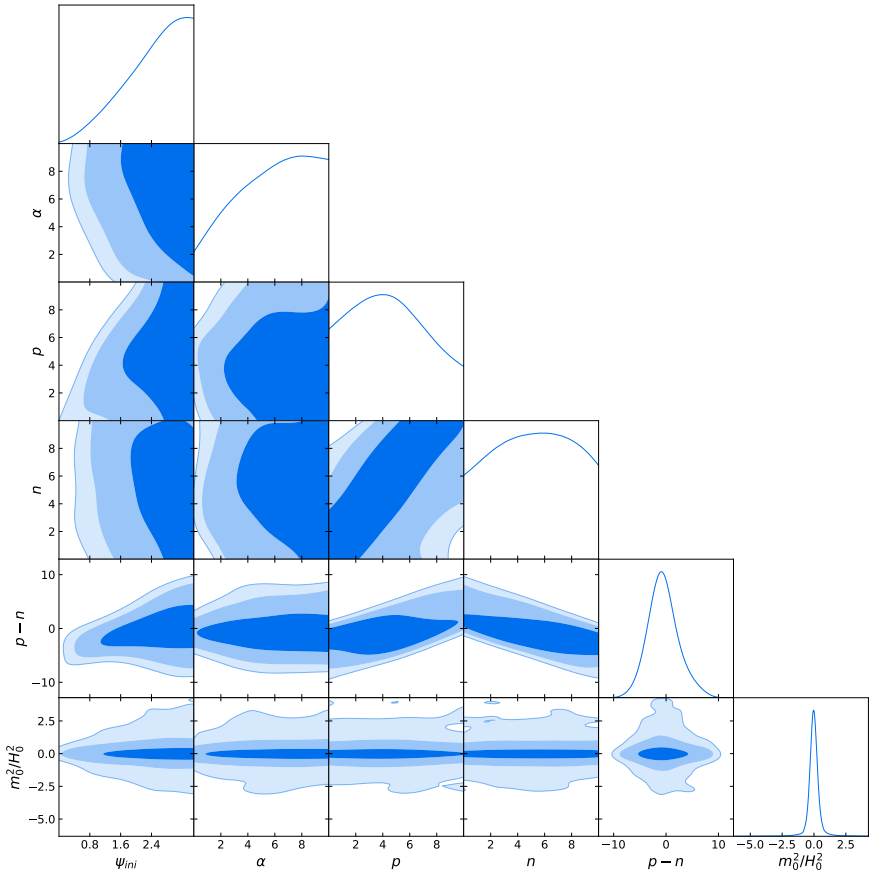

Figure 14: Posterior distribution for the generalized α-attractor dark energy model with potential 2.1. The contours show the confidence levels up to 99.7% CL, with darker colors for more probable results. The quantitative results are summarized in table 3.

from a conformal transformation but from gauge fixing the extra degree of freedom associated to the conformal symmetry of the inflationary Lagrangian. This model is appealing because it is able to interpolate between the two most common α-attractor forms used for inflation – the Starobinsky model and the T-model – and also interpolate between power law potential and ΛCDM dark energy regimes at low and high ψ, respectively. This potential also allows, in theory, the existence of clustering dark energy due to tachyonic solutions.

We can summarize the key points of this paper in the following ideas:

- The model is mainly described by its background evolution, which depends on the parameters in the following way:
  - At viably high ψ, it is in the thawing class, with the field excursion related to the equation of state and the α parameter as $\Delta\psi \sim \sqrt{1+w_0}/\sqrt{\alpha}$ and $1 + w_0 \sim 1/\alpha$ so $\Delta\psi \sim 1/\alpha$.
  - If $p > n$, the field always decreases and its speed is also inversely related to ψ_{ini}. In addition, p controls the steepness of the transition regime.
  - If $p < n$, the field can grow towards an asymptotic de Sitter state at infinity if $\psi_{ini} > \psi_{max}$. Around the inflection points, or too close to $\psi = 0$, the field evolution

is fast. The exponent n controls the height of the maximum, and the difference $p - n$ controls the characteristic scale of the uplifted exponential potential.

- The MCMC analysis showed that the ΛCDM-like regime is favored by the combined data set of Planck 2015 [15], BAO DR12 [16] and $E(z)$ estimation from supernovae [17]:
  - Both the initial field ψ_{ini} and α are pushed to larger values, where the field lingers on the plateau.
  - The case where $p \sim n$ is also favored as it keeps the potential from being too steep (the deviation from a flat plateau becomes second order in the uplifted exponential potential).
  - The tachyonic solutions compatible with the observations have a very mild instability that does not give appreciable dark energy clustering. They are, however, as likely as non-tachyonic ones: $m_0^2/H_0^2 = -0.01^{+0.97}_{-0.87}$.

We studied the properties of the model and its dependence on the different parameters. We saw that a better variable to understand the field evolution is $\psi = \phi/\sqrt{\alpha}$ instead of ϕ. The kinetic coefficient α (which for inflation models is intimately tied to the geometry of the superconformal field theory space) scales the field so that it determines at what value the field thaws. On the other hand, the reason why one has to consider both ψ and α is that the latter appears explicitly in the potential (but not kinetic) energy, in the frame in which the kinetic term is canonical (equation 1.3), so that different values of α yield different universe histories. In particular, we saw that the field evolution rate is inversely related to α – higher values of α slow it down. We showed how the initial position of the field ψ_{ini} played an important role determining how the field would evolve and had to be taken into account. For $p > n$ the field would always roll down but its speed would also decrease as ψ_{ini} grows, placing the field further on the plateau. On the contrary, when $p < n$ the potential has a maximum whose height and position is controlled by the relative size of n and p. In this scenario, the field could roll down towards $\psi = 0$, where the potential behaves like a power law potential $V \propto \phi^p$ (equation 2.2) or towards $\psi = \infty$, a de Sitter attractor with $V \propto 2^{-2n}$ (equation 2.3), with speed dependent on the proximity to the inflection points, where the force felt by the field is maximal. This correlates the expansion history with the field mass squared, and with its sign (which depends on which side of the inflection point the field is at present). In particular we have seen (figure 13) that the equation of state parameters w_0 and w_a are ordered so that for a given w_0 the higher mass squared gives higher w_a.

In section 2.3 we briefly studied how the negative mass squared could affect the observables. We saw that it would only have an effect if $|m^2|/H^2 \gtrsim k^2/(a^2H^2) > 1$ (equation 2.8), which greatly constrains the relevant modes, leaving just those of order $k \sim 10^{-3}\,\mathrm{Mpc}^{-1}$. Numerically, we studied the most extreme case we had obtained, that with $m^2/H_0^2 \sim -20$. In this case, we saw the mass term became relevant at $z \sim 3$ and that it was just today when it reaches the same order as the mode $k = 10^{-3}\,\mathrm{Mpc}^{-1}$. Therefore, the dark energy density perturbations are not appreciably influenced by the tachyonic instability, except possibly in the future.

For a detailed analysis we constrained the parameter space with MCMC for two α-attractor models. We compared our theoretical predictions with current datasets of CMB (Planck 2015 compressed likelihood [15]), BAO (BOSS DR12 [16]) and Supernovae (Pantheon + Hubble Space Telescope compressed [17, 26]). We also discussed how to choose priors since

as some parameters get large the models become insensitive to them and indistinguishable from ΛCDM.

The results for the two models were discussed in sections 3.3 and 3.4. The first case corresponds to the particular case where the potential is Starobinsky-like but leaving free the α parameter; i.e. fixing $p = 2$ and $n = 1$. We saw that the preferred models are those closer to ΛCDM and the best-fit is almost $w = -1$. Indeed the w_0–w_a behavior closely follows that of thawing dark energy for ψ_{ini} not too small, and this is bounded from below. Furthermore, the other cosmological parameters are compatible with those from Planck 2015 for ΛCDM.

These behaviors hold for the full generalized α-attractor model, with parameters α, p, n. The preferred region continued to be that closer to ΛCDM, and a new way of attaining that was for p and n to be nearly the same. Even though the model had much more freedom, the $w_0 - w_a$ behavior (figure 13b) still followed the thawing fit $w_a = -1.6(1 + w_0)$ quite well.

In closing, we would like to comment on possible future work based on this model. In this work, we have just studied a quintessence cosmological model, leaving aside the inflation epoch from which it is originally inspired and justified the absence of coupling to matter, even in the Starobinsky potential. Therefore, it is sensible to think of the next work as an investigation of the joint predictions of this generalized model over the whole history of the Universe, from inflation to late time cosmology. This kind of work would be in the spirit of the recent papers on the subject [5–7] and might show that this model is well suited to address both inflation and dark energy from a common physical mechanism, linking two of the fundamental problems in modern cosmology.

Acknowledgments

CGG would like to thank his UCM colleagues José M. Sánchez Velázquez, Héctor Villarrubia-Rojo and Miguel Aparicio Resco for useful discussions. We thank Renata Kallosh for interesting discussions. CGG and PRL are supported by AYA2015-67854-P from the Ministry of Industry, Sciece and Innovation of Spain and the FEDER funds. CGG is supported by the Spanish grant BES-2016-077038. EL is supported in part by the Energetic Cosmos Laboratory and by the U.S. Department of Energy, Office of Science, Office of High Energy Physics, under Award DE-SC-0007867 and contract no. DE-AC02- 05CH11231. MZ is supported by the Marie Sklodowska-Curie Global Fellowship Project NLO-CO. This paper is based upon work from COST action CA15117 (CANTATA), supported by COST (European Cooperation in Science and Technology)

References

[1] M. Galante, R. Kallosh, A. Linde, and D. Roest, *Unity of Cosmological Inflation Attractors*, *Phys. Rev. Lett.* **114** (2015), no. 14 141302, [arXiv:1412.3797].

[2] **WMAP** Collaboration, G. Hinshaw et al., *Nine-Year Wilkinson Microwave Anisotropy Probe (WMAP) Observations: Cosmological Parameter Results*, *Astrophys. J. Suppl.* **208** (2013) 19, [arXiv:1212.5226].

[3] **Planck** Collaboration, P. A. R. Ade et al., *Planck 2015 results. XX. Constraints on inflation*, *Astron. Astrophys.* **594** (2016) A20, [arXiv:1502.02114].

[4] R. Kallosh and A. Linde, *Universality Class in Conformal Inflation*, *JCAP* **1307** (2013) 002, [arXiv:1306.5220].

[5] K. Dimopoulos and C. Owen, *Quintessential Inflation with α-attractors*, *JCAP* **1706** (2017), no. 06 027, [arXiv:1703.00305].

[6] K. Dimopoulos and C. Owen, *Instant Preheating in Quintessential Inflation with α-Attractors*, arXiv:1712.01760.

[7] Y. Akrami, R. Kallosh, A. Linde, and V. Vardanyan, *Dark energy, α-attractors, and large-scale structure surveys*, arXiv:1712.09693.

[8] E. V. Linder, *Dark Energy from α-Attractors*, *Phys. Rev.* **D91** (2015), no. 12 123012, [arXiv:1505.00815].

[9] M. Shahalam, R. Myrzakulov, S. Myrzakul, and A. Wang, *Observational constraints on the generalized α attractor model*, *Int. J. Mod. Phys.* **D27** (2018) 1850058, [arXiv:1611.06315].

[10] S. Bag, S. S. Mishra, and V. Sahni, *New tracker models of dark energy*, arXiv:1709.09193.

[11] S. S. Mishra, V. Sahni, and Y. Shtanov, *Sourcing Dark Matter and Dark Energy from α-attractors*, *JCAP* **1706** (2017), no. 06 045, [arXiv:1703.03295].

[12] A. A. Starobinsky, *A New Type of Isotropic Cosmological Models Without Singularity*, *Phys. Lett.* **91B** (1980) 99–102.

[13] S. D. Odintsov and V. K. Oikonomou, *Inflationary α-attractors from $F(R)$ gravity*, *Phys. Rev.* **D94** (2016), no. 12 124026, [arXiv:1612.01126].

[14] T. Miranda, J. C. Fabris, and O. F. Piattella, *Reconstructing a $f(R)$ theory from the α-Attractors*, *JCAP* **1709** (2017), no. 09 041, [arXiv:1707.06457].

[15] **Planck** Collaboration, P. A. R. Ade et al., *Planck 2015 results. XIV. Dark energy and modified gravity*, *Astron. Astrophys.* **594** (2016) A14, [arXiv:1502.01590].

[16] **BOSS** Collaboration, S. Alam et al., *The clustering of galaxies in the completed SDSS-III Baryon Oscillation Spectroscopic Survey: cosmological analysis of the DR12 galaxy sample*, *Mon. Not. Roy. Astron. Soc.* **470** (2017), no. 3 2617–2652, [arXiv:1607.03155].

[17] A. G. Riess et al., *Type Ia Supernova Distances at $z > 1.5$ from the Hubble Space Telescope Multi-Cycle Treasury Programs: The Early Expansion Rate*, arXiv:1710.00844.

[18] B. Whitt, *Fourth Order Gravity as General Relativity Plus Matter*, *Phys. Lett.* **145B** (1984) 176–178.

[19] K.-i. Maeda, *Inflation as a Transient Attractor in R^2 Cosmology*, *Phys. Rev.* **D37** (1988) 858.

[20] J. D. Barrow, *The Premature Recollapse Problem in Closed Inflationary Universes*, *Nucl. Phys.* **B296** (1988) 697–709.

[21] D. Blas, J. Lesgourgues, and T. Tram, *The Cosmic Linear Anisotropy Solving System (CLASS) II: Approximation schemes*, *JCAP* **1107** (2011) 034, [arXiv:1104.2933].

[22] M. Zumalacárregui, E. Bellini, I. Sawicki, J. Lesgourgues, and P. G. Ferreira, *hi_class: Horndeski in the Cosmic Linear Anisotropy Solving System*, *JCAP* **1708** (2017), no. 08 019, [arXiv:1605.06102].

[23] R. N. Cahn, R. de Putter, and E. V. Linder, *Field Flows of Dark Energy*, *JCAP* **0811** (2008) 015, [arXiv:0807.1346].

[24] E. V. Linder, *Quintessence's last stand?*, *Phys. Rev.* **D91** (2015) 063006, [arXiv:1501.01634].

[25] P. Peter and J.-P. Uzan, *Primordial Cosmology*, p. 708. Oxford Graduate Texts. Oxford University Press, first ed., 2009.

[26] D. M. Scolnic et al., *The Complete Light-curve Sample of Spectroscopically Confirmed Type Ia Supernovae from Pan-STARRS1 and Cosmological Constraints from The Combined Pantheon Sample*, arXiv:1710.00845.

[27] **BOSS** Collaboration, T. Delubac et al., *Baryon acoustic oscillations in the Lyα forest of BOSS DR11 quasars*, *Astron. Astrophys.* **574** (2015) A59, [arXiv:1404.1801].

[28] J. Evslin, *Isolating the Lyman Alpha Forest BAO Anomaly*, *JCAP* **1704** (2017) 024, [arXiv:1604.02809].

[29] G. Efstathiou and J. R. Bond, *Cosmic confusion: Degeneracies among cosmological parameters derived from measurements of microwave background anisotropies*, *Mon. Not. Roy. Astron. Soc.* **304** (1999) 75–97, [astro-ph/9807103].

[30] B. Audren, J. Lesgourgues, K. Benabed, and S. Prunet, *Conservative Constraints on Early Cosmology: an illustration of the Monte Python cosmological parameter inference code*, *JCAP* **1302** (2013) 001, [arXiv:1210.7183].

[31] J. Akeret, S. Seehars, A. Amara, A. Refregier, and A. Csillaghy, *CosmoHammer: Cosmological parameter estimation with the MCMC Hammer*, arXiv:1212.1721.

[32] D. Foreman-Mackey, D. W. Hogg, D. Lang, and J. Goodman, *emcee: The mcmc hammer*, *PASP* **125** (2013) 306–312, [arXiv:1202.3665].

[33] J. Goodman and J. Weare, *Ensemble samplers with affine invariance*, *Communications in applied mathematics and computational science* **5** (2010), no. 1 65–80.

[34] **Planck** Collaboration, P. A. R. Ade et al., *Planck 2015 results. XIII. Cosmological parameters*, *Astron. Astrophys.* **594** (2016) A13, [arXiv:1502.01589].

[35] H. Akaike, *A new look at the statistical model identification*, *IEEE Transactions on Automatic Control* **19** (1974), no. 6 716–723.

[36] **DESI** Collaboration, A. Aghamousa et al., *The DESI Experiment Part I: Science,Targeting, and Survey Design*, arXiv:1611.00036.

[37] L. Amendola et al., *Cosmology and Fundamental Physics with the Euclid Satellite*, arXiv:1606.00180.

[38] R. Hounsell et al., *Simulations of the WFIRST Supernova Survey and Forecasts of Cosmological Constraints*, arXiv:1702.01747.